Progress In Electromagnetics Research, Vol. 122, 29–45, 2012

THREE-DIMENSIONAL MAGNETIC INDUCTION TOMOGRAPHY IMAGING USING A MATRIX FREE KRYLOV SUBSPACE INVERSION ALGORITHM

H. Y. Wei and M. Soleimani*

Department of Electronics and Electrical Engineering, University of Bath, Claverton Down, Bath BA2 7AY, UK

Abstract—Magnetic induction tomography (MIT) attempts to image the passive electromagnetic properties (PEP) of an object by measuring the mutual inductances between pairs of coils placed around its periphery. In recent years, there has been an increase in applications of non-contact magnetic induction tomography. When finite element-based reconstruction methods are used, that rely on the inversion of a derivative operator, the large size of the Jacobian matrix poses a challenge since the explicit formulation and storage of the Jacobian matrix could be in general not feasible. This problem is aggravated further in applications for example when the number of coils is increased and in three-dimension. Krylov subspace methods such as conjugate gradient (CG) methods are suitable for such large scale inverse problems. However, these methods require use of the Jacobian matrix, which can be large scale. This paper presents a matrix-free reconstruction method, that addresses the problems of large scale inversion and reduces the computational cost and memory requirements for the reconstruction. The idea behind the matrix-free method is that information about the Jacobian matrix could be available through matrix times vector products so that the creation and storage of big matrices can be avoided. Furthermore the matrix vector multiplications were performed in multiple core fashion so that the computational time can decrease even further. The method was tested for the simulated and experimental data from lab experiments, and substantial benefits in computational times and memory requirements have been observed.

Received 15 September 2011, Accepted 22 October 2011, Scheduled 8 November 2011

* Corresponding author: Manuchehr Soleimani (m.soleimani@bath.ac.uk).

1. INTRODUCTION

Magnetic induction tomography (MIT) is a new modality for medical, industrial and geophysical imaging [1–3], in which the impedance distribution within a medium is computed based on measurements of the mutual inductances between pairs of coils placed around the medium. One key advantage is its contact-less nature, which makes the technique of interest for non-invasive and non-intrusive applications.

Measurements are acquired by passing an alternating current through excitation coils, producing a primary magnetic field. This magnetic field interacts with conductive and permeable objects in the medium to produce eddy currents, which, in turn, produce a secondary magnetic field, which is measured by sensing coils. As the secondary field depends on the materials present, the measured induced voltage is a non-linear function of the electrical and magnetic properties of the medium, i.e., conductivity. MIT is a difficult problem for several reasons: 1) the secondary fields are very small compared to the primary for weakly conducting objects (such as geophysical and biological tissue); 2) measured data are very sensitive to artifacts due to sensor movement, and nearby conductive objects; 3) the mathematical problem is highly ill-posed and non-linear [1, 4].

Most of the MIT systems at this stage are still in two-dimensional scale [5, 6], which do not consume much of computational memory. Future trend of MIT imaging shows that in the near future many applications of MIT will move to 3D and large scale inverse problems. So, the authors believe that large inversion scaled MIT will soon be widely implemented into many industrial applications, as it is the case in geophysical applications, where many transmitters and receivers are involved. In addition, multi-frequency and rotational MIT are being developed for various applications with different bandwidth sensitivity. Simultaneous reconstruction of all passive electromagnetic properties is feasible as shown in [7] and that would mean the size of the inverse problem will increase by a factor of two or three. The same will be true for anisotropic MIT or 4D image reconstruction, including the time domain will massively increase the size of the inverse problems [8]. In all these cases the amount of memory requirement for inversion calculation will increase significantly, therefore iterative methods become more suitable techniques for large scale computation. The same problem may occur in a number of other inverse problems [9–15].

In this paper, results are presented in 3D imaging of electrical conductivity imaging using both simulated and experimental data. However, the results of the paper will be valid for all of the above

large scale inversions in MIT imaging. Three dimensional MIT enables volumetric image reconstruction from magnetic induction data. The conjugate gradients (CG) algorithm and its variants can be used to solve linear systems of equations $\mathbf{Kf} = \mathbf{b}$ and linear least squares problems $\min_{\mathbf{f}} \|\mathbf{b} - \mathbf{Kf}\|_2$, especially when the matrix $\mathbf{K}$ is very large scale. In 3D MIT reconstruction, the main computational challenge is that the matrix $\mathbf{K}$ usually is very large, and storing it in full requires an amount of memory well beyond the reach of commercial computers. In this paper, to overcome this difficulty, the matrix $\mathbf{K}$ is partitioned and stored blockwise, and blockwise matrix-vector multiplication are implemented within conjugate gradients least square (CGLS). It is worth noticing that there are several Krylov subspace methods that can be used for large scale MIT image reconstruction, such as generalized minimum residual (GMRES), quasi minimal residual (QMR) and biconjugate gradient stabilized (BiCGSTAB). The blockwise algorithms developed for CGLS can be adapted into these methods. This implementation allows the full access of the Jacobian matrix $\mathbf{K}$ for MIT reconstruction without further enhancing computer memory requirement.

2. FORWARD PROBLEM

The forward problem is a general eddy current problem where edge finite element method is used for discretisation. Edge FEM in terms of magnetic vector potential ($\mathbf{A}$) is used to simulate the forward eddy current problem [16, 17]. Validation of the forward model has been done in a previous study. Given $\mathbf{E} = -i\omega\mathbf{A}$ and $\mathbf{B} = \nabla \times \mathbf{A}$ we have

$$\nabla \times (\nu \nabla \times \mathbf{A}) + i\omega\sigma\mathbf{A} = \mathbf{J_s} \tag{1}$$

where $\nu = 1/\mu$, σ is electrical conductivity and ω is angular frequency. Edge FEM has some promising advantages compared with the more conventional nodal FEM for vector field computations. In edge FEM a vector field is represented using a basis of vector valued functions. Nodal FEM was used for the vector fields in electromagnetic. Although nodal FEM is easy and straightforward and its outcome accurate, several serious problems have been identified when the ordinary nodal-based finite elements were employed to compute vector electric or magnetic fields.

Galerkin's approximation using edge element basis functions yields

$$\int_{\Omega} (\nabla \times \mathbf{N}\nu\nabla \times \mathbf{A}) dx^3 + \int_{\Omega_e} (i\omega\sigma\mathbf{NA}) dx^3 = \int_{\Omega_c} (N\mathbf{J_s}) dx^3 \tag{2}$$

where $\mathbf{N}$ is any linear combination of edge basis functions, Ω is the entire region, Ω_e the eddy current region, and Ω_c the current source region.

In [17], the coil geometry needs to be considered when modeling the mesh, which makes the eddy current modeling more difficult and less flexible. In this paper, we define the current source by electric vector potential $\mathbf{J_s} = \nabla \times \mathbf{T_s}$. By doing this, the coil geometry modeling in the finite element mesh can then be eliminated by defining $\mathbf{T_s} = \mathbf{H_s}$, where $\mathbf{H_s}$ is the field of the coils in free space. The magnetic field $\mathbf{H_s}$ can be calculated using the Biot-Savart law. Let us denote by L_i the nodal scalar basis function. In edge FEM on a tetrahedral mesh a vector field is represented using a basis of vector valued functions, where N_{ij} associated with the edge between nodes i and j is $\mathbf{N}_{ij} = L_i \nabla L_j - L_j \nabla L_i$. The induced voltage in excitation coil can be calculated by

$$V_m = -\frac{i\omega}{I_0} \int_{\Omega_c} \mathbf{A} \cdot \mathbf{J_0} dx^3 \tag{3}$$

where $\mathbf{J_0}$ is a virtual current density with total current of I_0 passing through the coil, and $\mathbf{A}$ is the sum of the freespace magnetic vector potential and the magnetic potential calculated from Equation (2).

2.1. Sensitivity Analysis

Using the shape function and edge elements $\mathbf{N}_e$, the potential $\mathbf{A}$ inside each element can be expressed as $\mathbf{A} = \mathbf{N}_e \mathbf{A}_e$, where $\mathbf{A}_e$ are defined along edges [18].

With that the sensitivity term for each element as follows

$$\frac{\partial V_{ij}}{\partial \sigma_k} = -\frac{\omega^2}{I_i I_j} \mathbf{A}_e^i \left(\int_{\Omega_{ek}} \mathbf{N}_e \cdot \mathbf{N}_e^T dx^3 \right) (\mathbf{A}_e^j)^T \tag{4}$$

Equation (4) gives us sensitivity of the induced voltage pairs of coils of i, j with respect to an element, Ω_{ek} is the volume of element number k, I_i and I_j are excitation currents for the coils. Each row of the Jacobian matrix will be sensitivity of a given measured voltage over the changes in conductivity. Figure 1 shows the sensitivity map result of a double layer, 16 channel MIT system. All the coils are located around a 16 cm diameter cylindrical imaging area, where eight coils are situated at the top layer ($z = +5$) and the other eight coils are at the bottom layer ($z = -5$). The sensitivity map will be used for image reconstruction in Section 5.1.

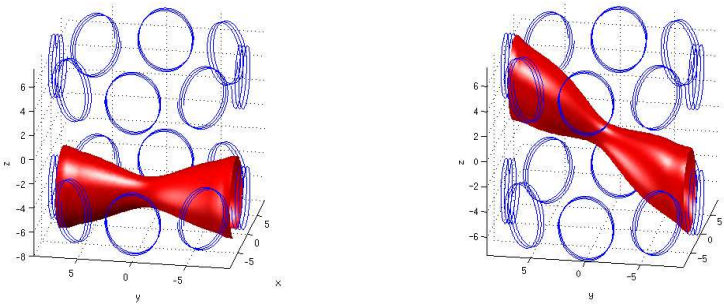

(a) (b)

Figure 1. Sensitivity map coupling between (a) coil 1 (bottom layer) and coil 5 (bottom layer) and (b) coil 1 (bottom layer) and coil 13 (top layer). All the x, y and z directions are in cm.

3. INVERSE PROBLEM

A regularized Gauss-Newton is the most commonly used method to solve the inverse MIT problem. Let V_m be the voltage measurement data, and F is a forward operator, which takes the vector of degree of freedom in the conductivity σ and calculates the corresponding voltages. The inverse solver is an optimization algorithm that finds a σ to minimize a suitable error functional. Reformulation of the inverse problem to include prior information is known as regularization and it can be expressed as minimization of the function

$$\| V_m - F(\sigma) \|^2 + G(\sigma) \tag{5}$$

where $G(\sigma)$ is a penalty term that can be implemented in discrete form using a regularizati on matrix. The Jacobian matrix $\mathbf{K}$ is a discretisation of $F^{'}(\sigma)$. In the non-linear steps, the Jacobian matrix will be updated throughout the iterations. In this paper, we focus on the linearised inverse problem $\mathbf{Kf} = \mathbf{b}$, where $\mathbf{K}$ is the Jacobian matrix, $\mathbf{f}$ is the conductivity distribution and $\mathbf{b}$ is the voltage measurement. Since $\mathbf{K}$ is ill-posed, Tikhonov regularisation term is required to solve the linearised problem

$$\delta\sigma = \left(\mathbf{K}^T\mathbf{K} + \alpha^2\mathbf{R}^T\mathbf{R}\right)^{-1}\left(\mathbf{K}^T\mathbf{b}\right) \tag{6}$$

where α is the regularisation parameter, $\mathbf{R}$ is the regularisation matrix and our $\mathbf{b}$ is the normalised measurement $\frac{V_m - V_0}{V_0}$ (V_0 is the background

voltage). In this case of Tikhonov regularisation, $\mathbf{R}^T\mathbf{R} = \mathbf{I}$, identity matrix.

The main challenges with this type of inverse technique, especially in a large scaled problem, is that a tremendous amount of memory is required to solve the $\mathbf{K}^T\mathbf{K}$ calculation and to store the matrix result. Some alternative inverse methods are required to resolve the limited memory issue [19, 20]. In [21], the CG method has been proposed for the large scale inversion of the electrical impedance tomography (EIT), however the Jacobian matrix needs to be loaded into computer memory.

3.1. Conjugate Gradient Least Squares

The main problem in large scale MIT algebraic reconstruction is that the matrix $\mathbf{K}$ is too big to solve by finding its inverse. The inverse techniques such as SVD or QR will require heavy memory resources and computational cost. However, iterative methods (Landweber or CG) can be used to avoid calculating $\mathbf{K}^\top\mathbf{K}$.

The CGLS method is one of the gradient based iterative algorithms for the numerical solution of particular systems of linear equations, whose matrix is symmetric and positive-definite. It can be applied to sparse systems that are too large to be handled by direct methods. Such systems often arise when numerically solving partial differential equations. CGLS is a variant of the CG method which can be used to solve the least square problem. In this paper, we are investigating the uses of this method for 3D MIT image reconstruction.

A MATLAB implementation of CGLS, the conjugate gradient method for unsymmetrical linear equations and least squares problems:

$$\mathbf{Kf} = \mathbf{b} \tag{7}$$

and minimise

$$\min_{\mathbf{f}} ||\mathbf{Kf} - \mathbf{b}|| \tag{8}$$

Since $\mathbf{K}^\top\mathbf{K}$ is positive-definite for any matrix $\mathbf{K}$, the conjugate gradient algorithm can be applied to the normal equations

$$\mathbf{K}^\top\mathbf{Kf} = \mathbf{K}^\top\mathbf{b} \tag{9}$$

where the $m \times n$ matrix $\mathbf{K}$ is the Jacobian matrix obtained by the forward projection, $\mathbf{f}$ is the scanned image and $\mathbf{b}$ is the measurement data. This is known as conjugate gradient least squares. The standard CGLS algorithm recipe is shown as follows:

Let $\mathbf{r_0} = \mathbf{b} - \mathbf{Kf_0}$ and $\mathbf{p_0} = \mathbf{M^{-1}r_0}$, where $\mathbf{M^{-1}}$ is the preconditional matrix

loop start

$$\mathbf{a_{k+1}} = \frac{\left\|\mathbf{K}^\top \mathbf{r_k}\right\|^2}{\left\|\mathbf{K}\mathbf{p_k}\right\|^2} \tag{10}$$

$$\mathbf{f_{k+1}} = \mathbf{f_k} + \mathbf{a_k}\mathbf{p_k} \tag{11}$$

$$\mathbf{r_{k+1}} = \mathbf{r_k} - \mathbf{a_k}\mathbf{K}\mathbf{p_k} \tag{12}$$

if ($r_{k+1} <$ **threshold**)

break;

else

$$\beta_\mathbf{n} = \frac{\left\|\mathbf{K}^\top \mathbf{r_{k+1}}\right\|^2}{\left\|\mathbf{K}^\top \mathbf{r_k}\right\|^2} \tag{13}$$

$$\mathbf{p_{k+1}} = \mathbf{K}^\top \mathbf{r_{k+1}} + \beta_\mathbf{n}\mathbf{p_k} \tag{14}$$

loop end

where $\mathbf{r_k}$ is the residual at the $\mathbf{k}$th step and $\mathbf{p_k}$ is an auxiliary vector of length n. With CGLS, the number of iterations provides the effect of regularisation to the final reconstructed image. However, it is unclear how many iterations should be performed in order to provide the optimal regularisation. The additional Tikhonov regularisation has been applied by adding an extra term in matrix $\mathbf{K}$.

$$\begin{bmatrix} \mathbf{K} \\ \\ \alpha\mathbf{I} \end{bmatrix} f = \begin{bmatrix} \mathbf{b} \\ \\ 0 \end{bmatrix}, \tag{15}$$

where α is the regularisation parameter and $\mathbf{I}$ is the sparse matrix with a size of $n \times n$. The new $\begin{bmatrix} \mathbf{K} \\ \alpha\mathbf{I} \end{bmatrix}$ matrix now has a dimension of $(m+n) \times n$.

3.2. Blockwise Matrix Vector Multiplication

As mentioned previously, due to the large memory required for storing a 3D matrix $\mathbf{K}$, only a fraction of the matrix could be used under the constraint of the current computer memory capacity. However, gradient based methods such as CGLS do not require access to the full matrix $\mathbf{K}$. All that is required is one matrix-vector multiplication with each of $\mathbf{K}$ and $\mathbf{K}^\top$ per iteration. Therefore, blockwise matrix-vector multiplication within CGLS provides a solution to our memory capacity constraints (even given a extremely large 3D matrix $\mathbf{K}$). The algorithm has the ability to handle the problem with a limited amount of memory, as it does not require the matrix $\mathbf{K}$ to be loaded all at once.

In addition, the matrix multiplications can be implemented to run in parallel, which could potentially increase the reconstruction speed dramatically.

In the CGLS algorithm, vector multiplications are required in Equations (12) and (14), which are $\mathbf{Kp}$ and $\mathbf{K}^\top\mathbf{r}$ respectively. In order to realise the blockwise CGLS method, the sensitivity matrix needs to be divided into blocks according to current computer memory capacity. Recall that the matrix $\mathbf{K}$ resulting from a 3D full data set, the matrix $\mathbf{K}$ can be divided into l segments,

$$\mathbf{K} = \begin{bmatrix} \mathbf{K}_1 \\ \mathbf{K}_2 \\ \vdots \\ \mathbf{K}_l \\ \mathbf{K}_{l+1} \end{bmatrix},$$

where the index j in $\mathbf{K}$ refers to the position of each block within the matrix $\mathbf{K}$. Each block $\mathbf{K}_j$ contains a set of precalculated sensitivity elements $\frac{\delta V_{ij}}{\delta \sigma}$, and itself has a dimension of m/l by n, except for $\mathbf{K}_{l+1}$, which is the $n \times n$ regularised identity matrix described in Equation (15) used for Tikhonov regularisation. Matrix-vector multiplications can then easily be implemented blockwise. In the case of $\mathbf{Kp}$ multiplication, $\mathbf{p}$ is a vector with size of $n \times 1$,

$$\mathbf{Kp} = \begin{bmatrix} \mathbf{K}_1\mathbf{p} \\ \mathbf{K}_2\mathbf{p} \\ \vdots \\ \mathbf{K}_l\mathbf{p} \\ \mathbf{K}_{l+1}\mathbf{p} \end{bmatrix},$$

where each $\mathbf{K}_j\mathbf{p}$ involves a matrix-vector multiplication with the block $\mathbf{K}_j$. Similarly, in the $\mathbf{K}^\top\mathbf{r}$ multiplication, if $\mathbf{r}$ has a vector dimension of $1 \times (m+n)$, it can be partitioned into blocks as well:

$$\mathbf{r} = \begin{bmatrix} \mathbf{r}_1 \\ \mathbf{r}_2 \\ \vdots \\ \mathbf{r}_l \\ \mathbf{r}_{l+1} \end{bmatrix},$$

where each $\mathbf{r}_j$ is a vector of length $(m+n)/l$, and the $\mathbf{K}^\top\mathbf{r}$ vector multiplication result becomes:

$$\mathbf{K}^\top\mathbf{r} = \sum_{j=1}^{l+1} \mathbf{K}_j^\top \mathbf{r}_j$$

Each blockwised sensitivity matrix $\mathbf{K}_j$ can be loaded during the matrix-vector multiplication. Furthermore, these vectors can be multiplied in parallel since each $\mathbf{K}_j^\top \mathbf{r}_j$ blockwised calculation is independent to each other, therefore the computation speed can be further enhanced if the computer has multiple cored CPU to handle the multiplication task simultaneously. Once the $\mathbf{Kp}$ and $\mathbf{K}^\top\mathbf{r}$ multiplications are complete, the equations in Section 3.2 makes it possible to run CGLS using the blockwised matrix $\mathbf{K}_j$.

4. EXPERIMENTAL SETUP

In general, electrical tomography such as MIT has a smaller amount of measurements compared to other types of tomography such as CT or fluorescence tomography [19]. In MIT, with a n_c channels system, $(n_c \times (n_c - 1))/2$ measurements will be collected to reconstruct one image. The scale of inverse problem only becomes significant when the problem becomes three-dimensional. In the following experiments, 3-D problems are solved using blockwised CGLS methods to validate its performance. The work station used for all computation works has a UNIX platform, eight cores CPU (3.16 GHz) with 15 GB RAM.

4.1. Simulation Setup

A two layers, 16 channels MIT system was simulated in this experiment. The imaging region has a diameter of 16 cm. All the sensor coils have a radius of 3 cm and are spread evenly around the cylindrical imaging area at different layers. Eight coil sensors are assigned into two layers, top and bottom. The distance between the top and the bottom sensor layers is 10 cm.

Using equations described in Section 2.1, the magnetic field coupling between different coils are shown in Figure 1. In order to demonstrate the performance of the CGLS method, a 3D sensitivity map is necessary and a large grid number was chosen: $81 \times 81 \times 81$. The storage size of this matrix dataset is 464 MB.

4.2. MIT System Setup

The MIT system Bath-Mk I was used to gather the real life data in this study. Bath MIT Mk-I is an eight channel MIT system which is mainly comprised of a sensor array, a CMOS multiplexer and a National Instrument based data acquisition card. The air cored coil was manually wounded around a cylindrical plastic template with copper wire of 50 turns and has a radius of 21 mm. The coil may act

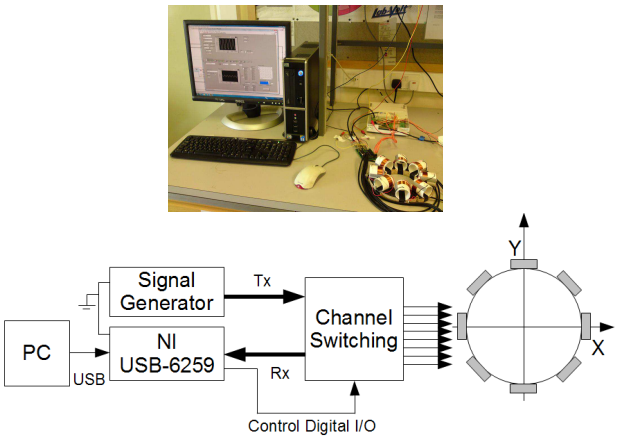

Figure 2. Block diagram of Bath MIT Mk I.

either a transmitter or a receiver, as determined by the PC controlled multiplexer. The sensors are placed equally at the periphery of a circular wooden base; thus creating an interaction angle of 45 degrees between adjacent coils for our eight channel system. The circular region for our MIT system is a circular space enclosed by coil arrays, with a diameter of 110 mm.

ADG406 multiplexers (Analog Devices, Inc.) are employed in our system to accomplish the channel switching processes. ADG406 is a 16-to-1, monolithic CMOS analogue multiplexer which has features of low 'ON' resistance and high input signal range. For the system presented in this paper, only 8 multiplexer channels are connected to coils. However, the full capacity of the multiplexers can be used if needed in order to expand the Bath MIT Mk-I to a two layer, three dimensional system. The 1.5 V p-p, 5 kHz sinusoidal signals are generated from a TOPWARD 8112 signal generator. The built-in LabView functions are used to measure the amplitude change of the detecting signal. Figure 2 shows the MIT system and its simplified block diagram.

5. RESULTS

5.1. Simulated Data

The reconstructed images of the simulated conductivity distribution are shown in Figures 4 and 5. The sensitivity map described in Section 4.1 was used in both cases for the matrix free CGLS inversion.

With a $(81 \times 81 \times 81)$ sensitivity matrix $\mathbf{K}$, the $\mathbf{K}^{\top}\mathbf{K}$ computation is very difficult for an ordinary computer, therefore in this section, only the CGLS method is used for image reconstruction. The simulated voltage data is generated from another set of mesh grid $(51 \times 51 \times 51)$ to avoid so called 'inverse crime'. A 1% noise of the measurement values were also introduced to the measurements.

For time comparison, the same CGLS algorithm was executed with 25 iterations using parallel computing and serial streaming computing respectively. The regularisation factor was chosen empirically and the optimal number of iterations were decided from the projection error graph (Figure 3). The projection error is the norm of the residual throughout the entire iteration process. As shown in the figure, once the number of iterations exceed a certain value, the image error will saturate towards a fixed value. Further increasing the number of iterations will not benefit the image accuracy.

The figures show that the location of the simulated targets in both cases were recovered successfully. However, the reconstructed images show a much 'smoother' surface than the true distribution. This is due to the regularisation effect mainly from the CGLS iterations and the penalty term $\mathbf{R}^{T}\mathbf{R}$, which provides a smoothing effect to the reconstructed images. It is also noticed that the regularisation effect to the reconstructed image is mainly dominated by the CGLS iteration, the Tikhonov regularisation factor has a minor effect to the inverse result. Furthermore, in Figure 4, the middle part of the reconstructed shape is observed to be irregular compared to the true image. This is because of the weaker sensitivity coupling in the middle area of the imaging space. As shown in Figure 1, the sensitivity coupling between two coils tends to be weaker at the centre area.

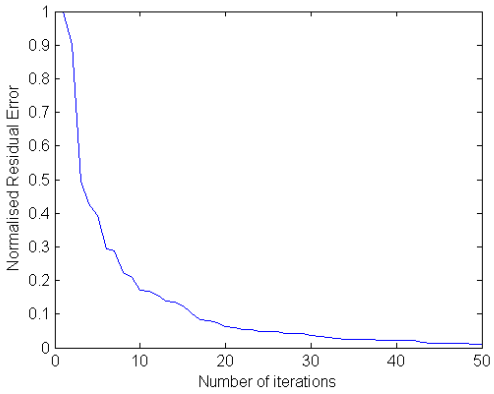

Figure 3. The convergence plot against the number of iterations.

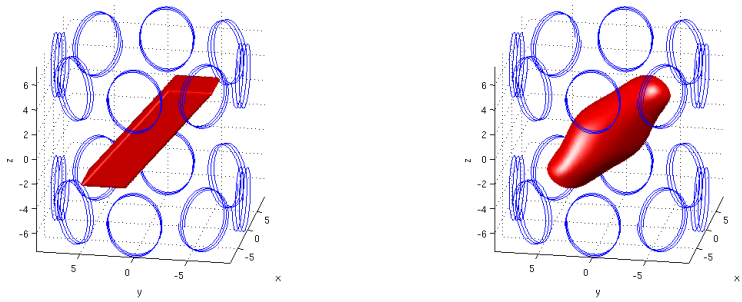

(a) (b)

Figure 4. Simulated data (a metallic rod lying diagonally across the imaging area) reconstruction using CGLS method. (a) The simulated image and (b) the reconstructed image. The computational time required for traditional se- rial computing was 192.44 seconds while for the reconstruction using parallel computing was 41.48 seconds.

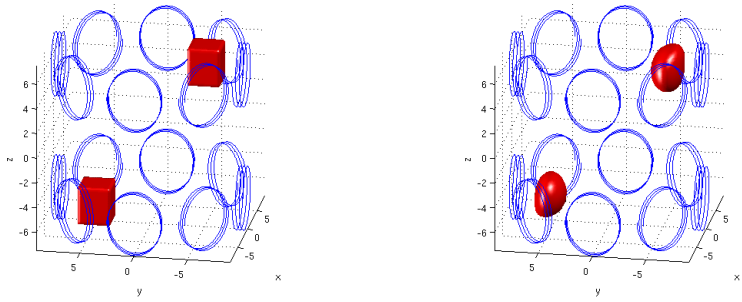

(a) (b)

Figure 5. Simulated data (two metallic cubes sitting on different levels of the imaging area) reconstruction using CGLS method. (a) The simulated image. (b) The reconstructed image. The computational time required for traditional serial computing was 192.51 seconds while for the reconstruction using parallel computing was 42.22 seconds.

5.2. Experimental Data

In this section, the measuring data were collected from a real eight channel MIT system. The images were also reconstructed by the blockwised CGLS method with the same size of the sensitivity map ($81 \times 81 \times 81$). Again, only the CGLS method is implemented because with this amount of dataset (28 measurements $\times 81^3$ image elements), it is still very difficult to perform the Tikhonov linear inversion and in particular $\mathbf{K}^\top \mathbf{K}$ calculation for a standard computer.

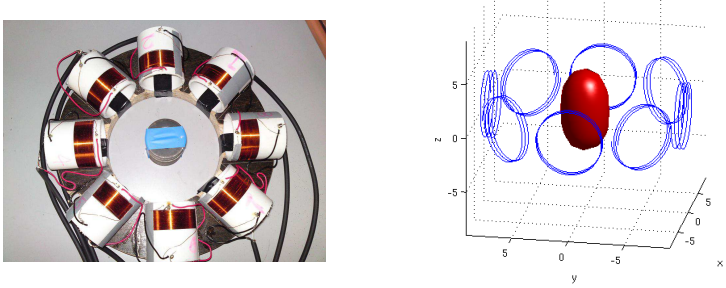

(a) (b)

Figure 6. (a) A single metal piece (4 cm height) at the centre of the imaging area, and (b) the reconstructed image from the data collected by Bath MIT Mk-I.

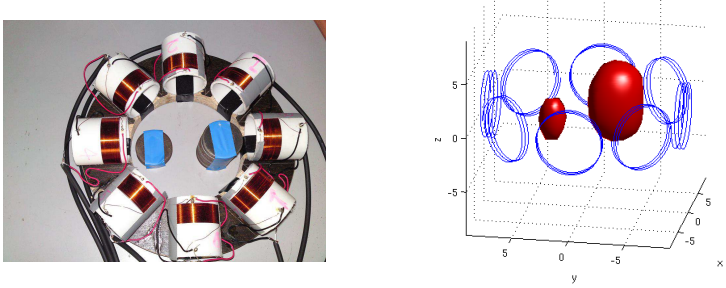

(a) (b)

Figure 7. (a) Two metal pieces with different height sitting within the imaging area, and (b) its reconstructed image from the data collected by Bath MIT Mk-I.

Figures 6 and 7 show the reconstruction result with different sizes of metal pieces in the imaging area. The heights of the metal pieces are 4 cm and 1 cm respectively. The number of CGLS iterations used to reconstruct the images was 25. The computational time for the parallel and serial execution was also calculate d for comparison.

The figures again show satisfied image results, the number and the size difference of the imaging objects are both correctly shown in the reconstructed figures.

5.3. Computational Time

By dividing the sensitivity matrix $\mathbf{K}$ into several segments, the computation memory requirement can be minimised. Furthermore,

the blockwised matrices allow us to utilise the parallel programming scheme in MATLAB to further enhance the calculation speed (if the computer is equipped with multiple-cores CPU). In this section, two experiments are performed to demonstrate the advantage of using parallel CGLS computing for image reconstruction. A single layer, 8 coils MIT system was used to gather the voltage reading on the coil, with high conductive objects presented within the region of interest.

Equation (4) is used to determine the sensitivity map **K**. The sensitivity map at this stage is constructed by tetrahedral mesh, which contains a huge amount of edge values. For the simplicity of the visualisation, the tetrahedral mesh needs to be converted into cubic mesh by using the 'tsearchn' function in MATLAB. The size of the cubic mesh can be varied by changing the input parameters. Here, the sensitivity map is divided into seven segments, and the cubic mesh sizes are set to $(21 \times 21 \times 21)$, $(51 \times 51 \times 51)$, $(81 \times 81 \times 81)$ and $(101 \times 101 \times 101)$ for comparison. The results shown in Table 1 indicate the time required to complete 25 CGLS iteration for one reconstructed image.

Now we divide the sensitivity matrix **K** into two segments only, then measure the computational time for a single reconstructed image (25 CGLS iterations) again. The result is shown in Table 2.

From both tables, it can be clearly seen that the computational speed of blockwised CGLS method can be improved substantially by using the parallel execution. However, this improvement only

Table 1. Time performance comparison with different three dimensional mesh size (seven segments).

	parallel execution	serial execution
$(21 \times 21 \times 21)$	3.04 s	2.05 s
$(51 \times 51 \times 51)$	6.38 s	12.90 s
$(81 \times 81 \times 81)$	26.92 s	44.20 s
$(101 \times 101 \times 101)$	33.82 s	80.69 s

Table 2. Time performance comparison with different three dimensional mesh size (two segments).

	parallel execution	serial execution
$(21 \times 21 \times 21)$	2.43 s	2.05 s
$(51 \times 51 \times 51)$	8.24 s	12.53 s
$(81 \times 81 \times 81)$	30.83 s	50.03 s
$(101 \times 101 \times 101)$	49.65 s	81.03 s

starts becoming significant when we expand the scale of the inverse problem. The larger the inverse problem size, the more benefit can be obtained from this blockwise algorithm. In particular in our 16 channel simulation example (120 measurements $\times 81^3$ image elements) in Section 5.1, the execution time becomes almost five times shorter than the ordinary CGLS method. The computational speed is also dependent of the amount of matrix segmentation. The number of segments needs to be equal or more than the number of CPU cores in order to achieve the optimum speed performance.

6. DISCUSSION AND CONCLUSION

Iterative methods are well studied in inverse problems such as MIT reconstruction. However, CG-type iterative methods are rarely investigated in this context. The main challenge in 3D MIT reconstruction is that the matrix $\mathbf{K}$ can usually be extremely large scale. Hence, the application of CGLS in MIT reconstruction was studied. In our numerical tests in Section 5, it can be clearly seen that CGLS was effective in solving the resulting large sparse least square problems, as the objects within the measuring space can all be identified correctly. The Tikhonov regularisation described in this paper contributes very smooth reconstruction results, which makes the edges of the true shape not very detectable. Some other regularisation techniques such as the Total Variation (TV) algorithm can be implemented in order to obtain a sharper reconstruction result, however, this is not within the scope of this paper.

In 3D image reconstruction, memory requirement is too large for commercial computer standards. Therefore, CGLS with blockwise matrix-vector multiplications was implemented. The Jacobian matrix $\mathbf{K}$ has been divided into blocks, allowing each block to be loaded blockwise sequentially or in parallel when needed at every iteration. This makes it possible to use the full matrix $\mathbf{K}$ for 3D MIT reconstruction without implementing the full matrix. Since each matrix-vector multiplication is independent to each other, partition ing the matrix $\mathbf{K}$ into blocks allows us to access several blocks of $\mathbf{K}$ simultaneously for the blockwise multiplication in CGLS. As a result, a faster reconstruction speed can be achieved. As shown Section 5.3, parallel computing execution can provide a faster reconstruction rate than using CGLS directly on a single block of $\mathbf{K}$ (serial execution). In the result section, the execution time of the parallel computing was found to be five times shorter for a double layer, 16 channels MIT system. By using this proposed algorithm, it allows the immediate use of the 3D MIT reconstruction in high performance computing. Also,

the advantage of dividing Jacobian matrix **K** according to computer memory capacity will enable the use of 3D MIT reconstruct ion for personal computer standards. It provides a good balance between the computational time and memory usage.

REFERENCES

1. Griffiths, H., "Magnetic induction tomography," *Institute of Physics Publishing Meas. Sci. Technol.*, Vol. 12, 1126–1131, Dec. 2001.
2. Ma, X., A. J. Peyton, S. R. Higson, A. Lyons, and S. J. Dickinson, "Hardware and software design for an electromagnetic induction tomography system applied to high contrast metal process applications," *Meas. Science and Technology*, Vol. 17, No. 1, 111–118, 2006.
3. Korjenevsky, A., V. Cherepenin, and S. Sapetsky, "Magnetic induction tomography: Experimental realization," *Physiol. Meas.*, Vol. 21, No. 1, 89–94, 2000.
4. Hanson, P. C., *Rank-deficient and Discrete Ill-posed Problems*, SIAM, 1998.
5. Peyton, A. J., Z. Z. Yu, and G. M. Lyon, "An overview of electromagnetic inductance tomography: Description of three different systems," *Measurement Science & Technology*, Vol. 7, No. 3, 261–271, Mar. 1996.
6. Watson, S., R. J. Williams, W. A. Gough, and H. Griffiths, "A magnetic induction tomography system for samples with conductivities less than $10\,\mathrm{s\ m^{-1}}$," *Meas. Sci. Technol.*, Vol. 19, 045501-11, 2008.
7. Soleimani, M., "Simultaneous reconstruction of permeability and conductivity in magnetic induction tomography," *Journal of Electromagnetic Waves and Applications*, Vol. 23, No. 5/6, 785–798, 2009.
8. Soleimani, M., N. Mitchell, R. Banasiak, R. Wajman, and A. Adler, "Four-dimensional electrical capacitance tomography imaging using experimental data," *Progress In Electromagnetics Research*, Vol. 90, 171–186, 2009.
9. Banasiak, R., R. Wajman, D. Sankowski, and M. Soleimani, "Three-dimensional nonlinear inversion of electrical capacitance tomography data using a complete sensor model," *Progress In Electromagnetics Research*, Vol. 100, 219–234, 2010.
10. Goharian, M., M. Soleimani, and G. R. Moran, "A trust region subproblem for 3D electrical impedance tomography inverse

problem using experimental data," *Progress In Electromagnetics Research*, Vol. 94, 19–32, 2009.

11. Catapano, I., F. Soldovieri, and L. Crocco, "On the feasibility of the linear sampling method for 3D GPR surveys," *Progress In Electromagnetics Research*, Vol. 118, 185–203, 2011.
12. Flores-Tapia, D., M. O'Halloran, and S. Pistorius, "A bimodal reconstruction method for breast cancer imaging," *Progress In Electromagnetics Research*, Vol. 118, 461–486, 2011.
13. Asimakis, N. P., I. S. Karanasiou, and N. K. Uzunoglu, "Non-invasive microwave radiometric system for intracranial applications: A study using the conformal L-notch microstrip patch antenna," *Progress In Electromagnetics Research*, Vol. 117, 83–101, 2011.
14. Litman, A., J. M. Geffrin, and H. Tortel, "On the calibration of a multistatic scattering matrix measured by a fixed circular array of antennas," *Progress In Electromagnetics Research*, Vol. 110, 1–21, 2010.
15. Parise, M., "Fast computation of the forward solution in controlled- source electromagnetic sounding problems," *Progress In Electromagnetics Research*, Vol. 111, 119–139, 2011.
16. Biro, O., "Edge element formulations of eddy current problems," *Comput. Methods Appl. Mech. Engrg.*, Vol. 169, 391–405, 1999.
17. Soleimani, M., "Sensitivity maps in three-dimensional magnetic induction tomography," *Insight*, Vol. 48, No. 1, 39–44, Jan. 2006.
18. Soleimani, M. and W. R. B. Lionheart, "Image reconstruction in three-dimensional magnetostatic permeability tomography," *IEEE Transactions on Magnetics*, Vol. 41, No. 4, 1274–1279, 2005.
19. Zacharopoulos, A. D., P. Svenmarker, J. Axelsson, M. Schweiger, S. R. Arridge, and S. Adndersson-Engels, "A matrix-free algorithm for multiple wavelength fluorescene tomography," *Optics Express*, Vol. 17, No. 5, 3025–3035, 2009.
20. Li, M., A. bubakar, J. Liu, G. Pan, and T. M. Habashy, "A compressed implicit jacobian scheme for 3D electromagnetic data inversion," *Geophysics*, Vol. 76, No. 3, F173–F183, 2011.
21. Polydorides, N., W. R. B. Lionheart, and H. McCann, "Krylov subspace iterative techniques: On the detection of brain activity with electrical impedance tomography," *IEEE Trans. Med. Imaging*, Vol. 21, 596–603, 2002.